Kloe Memo 00-215

June 2000

KLOE first results on hadronic physics

The KLOE collaboration

Abstract

The KLOE detector (1) at DAΦNE, the Frascati ϕ-factory, has started taking data in April 1999 and a total integrated luminosity of 2.4 pb^{-1} has been collected by the end of '99, corresponding to $\sim$8 millions ϕ decays. With these data a preliminary measurement of ϕ radiative decays $\phi \to \eta\gamma$, $\phi \to \pi^0\gamma$, $\phi \to \eta'\gamma$, $\phi \to \pi^0\pi^0\gamma$, $\phi \to \pi^+\pi^-\gamma$, $\phi \to \eta\pi^0\gamma$ and of the hadronic decay $\phi \to \pi^+\pi^-\pi^0$ has been performed. The energy spectrum of the radiated photon in case of the $\pi^0\pi^0\gamma$, $\pi^+\pi^-\gamma$, $\eta\pi^0\gamma$ final states allows us to extract the information on the contribution of the direct decays $\phi \to f_0\gamma$, $\phi \to a_0\gamma$. The measurement of BR($\phi \to f_0\gamma$), BR($\phi \to a_0\gamma$) can help in understanding the nature of $f_0(980)$ and $a_0(980)$ which is still under debate. The value of BR($\phi \to \eta'\gamma$) can be related to the gluonic content of the $\eta'(958)$ while the ratio R=BR($\phi \to \eta'\gamma$)/BR($\phi \to \eta\gamma$) can help in establishing the value of the $\eta - \eta'$ mixing angle θ_p.

Furthermore a high statistics analysis of the Dalitz plot in the $\phi \to \pi^+\pi^-\pi^0$ decay allows us to extract a possible contribution of the direct decay with respect to the dominant $\rho\pi$ mode and to obtain a new measurement of the parameters of the ρ line shape, including the $\rho^0 - \rho^\pm$ mass difference.

Contributed paper N.503 to the XXX International Conference on High Energy Physics,

Osaka 27 jul - 2 aug 2000.

M. Adinolfi,[m] A. Aloisio,[g] F. Ambrosino,[g] A. Andryakov,[f] A. Antonelli,[c] M. Antonelli,[c] F. Anulli,[c] C. Bacci,[n] A. Bankamp,[d] G. Barbiellini,[q] F. Bellini,[n] G. Bencivenni,[c] S. Bertolucci,[c] C. Bini,[k] C. Bloise,[c] V. Bocci,[k] F. Bossi,[c] P. Branchini,[n] S. A. Bulychjov,[f] G. Cabibbo,[k] A. Calcaterra,[c] R. Caloi,[k] P. Campana,[c] G. Capon,[c] G. Carboni,[m] A. Cardini,[k] M. Casarsa,[q] G. Cataldi,[d] F. Ceradini,[n] F. Cervelli,[j] F. Cevenini,[g] G. Chiefari,[g] P. Ciambrone,[c] S. Conetti,[r] E. De Lucia,[k] G. De Robertis,[a] R. De Sangro,[c] P. De Simone,[c] G. De Zorzi,[k] S. Dell'Agnello,[c] A. Denig,[d] A. Di Domenico,[k] C. Di Donato,[g] S. Di Falco,[j] A. Doria,[g] E. Drago,[g] V. Elia,[e] O. Erriquez,[a] A. Farilla,[n] G. Felici,[c] A. Ferrari,[n] M. L. Ferrer,[c] G. Finocchiaro,[c] C. Forti,[c] A. Franceschi,[c] P. Franzini,[k,i] M. L. Gao,[b] C. Gatti,[c] P. Gauzzi,[k] S. Giovannella,[c] V. Golovatyuk,[e] E. Gorini,[e] F. Grancagnolo,[e] W. Grandegger,[c] E. Graziani,[n] P. Guarnaccia,[a] U. v. Hagel,[d] H. G. Han,[b] S. W. Han,[b] X. Huang,[b] M. Incagli,[j] L. Ingrosso,[c] Y. Y. Jiang,[b] W. Kim,[o] W. Kluge,[d] V. Kulikov,[f] F. Lacava,[k] G. Lanfranchi,[c] J. Lee-Franzini,[c,o] T. Lomtadze,[j] C. Luisi,[k] C. S. Mao,[b] M. Martemianov,[f] A. Martini,[c] M. Matsyuk,[f] W. Mei,[c] L. Merola,[g] R. Messi,[m] S. Miscetti,[c] A. Moalem,[h] S. Moccia,[c] M. Moulson,[c] S. Mueller,[d] F. Murtas,[c] M. Napolitano,[g] A. Nedosekin,[c,f] M. Panareo,[e] L. Pacciani,[m] P. Pagès,[c] M. Palutan,[m] L. Paoluzi,[m] E. Pasqualucci,[k] L. Passalacqua,[c] M. Passaseo,[k] A. Passeri,[n] V. Patera,[l,c] E. Petrolo,[k] G. Petrucci,[c] D. Picca,[k] G. Pirozzi,[g] C. Pistillo,[g] M. Pollack,[o] L. Pontecorvo,[k] M. Primavera,[e] F. Ruggieri,[a] P. Santangelo,[c] E. Santovetti,[m] G. Saracino,[g] R. D. Schamberger,[o] C. Schwick,[j] B. Sciascia,[k] A. Sciubba,[l,c] F. Scuri,[q] I. Sfiligoi,[c] J. Shan,[c] P. Silano,[k] T. Spadaro,[k] S. Spagnolo,[e] E. Spiriti,[n] C. Stanescu,[n] G. L. Tong,[b] L. Tortora,[n] E. Valente,[k] P. Valente,[c] B. Valeriani,[j] G. Venanzoni,[d] S. Veneziano,[k] Y. Wu,[b] Y. G. Xie,[b] P. P. Zhao,[b] Y. Zhou[c]

[a] Dipartimento di Fisica dell'Università e Sezione INFN, Bari, Italy.
[b] Institute of High Energy Physics of Academica Sinica, Beijing, China.
[c] Laboratori Nazionali di Frascati dell'INFN, Frascati, Italy.
[d] Institut für Experimentelle Kernphysik, Universität Karlsruhe, Germany.
[e] Dipartimento di Fisica dell'Università e Sezione INFN, Lecce, Italy.
[f] Institute for Theoretical and Experimental Physics, Moscow, Russia.
[g] Dipartimento di Scienze Fisiche dell'Università e Sezione INFN, Napoli, Italy.
[h] Physics Department, Ben-Gurion University of the Negev, Israel.
[i] Physics Department, Columbia University, New York, USA.
[j] Dipartimento di Fisica dell'Università e Sezione INFN, Pisa, Italy.
[k] Dipartimento di Fisica dell'Università e Sezione INFN, Roma I, Italy.
[l] Dipartimento di Energetica dell'Università, Roma I, Italy.
[m] Dipartimento di Fisica dell'Università e Sezione INFN, Roma II, Italy.
[n] Dipartimento di Fisica dell'Università e Sezione INFN, Roma III, Italy.
[o] Physics Department, State University of New York at Stony Brook, USA.
[q] Dipartimento di Fisica dell'Università e Sezione INFN, Trieste/Udine, Italy.
[r] Physics Department, University of Virginia, USA.
* Associate member

Model	BR($\phi \to f_0\gamma$)
$s\bar{s}(^3P_0)$	$\sim 10^{-5}$
$(u\bar{u}+d\bar{d})/\sqrt{2}(^3P_0)$	$\leq 10^{-6}$
$q\bar{q}q\bar{q}$	$\sim 10^{-4}$
$K\bar{K}$ molecule	$10^{-4} \div 10^{-5}$

Table 1: Theoretical predictions for $\phi \to f_0\gamma$.

1 Introduction

1.1 Radiative decays

1.1.1 The scalar sector: $\phi \to f_0\gamma$, $\phi \to a_0\gamma$

The lightest scalar mesons, with masses below 1 GeV, have defied classification for nearly half a century. The narrow states $f_0(980)$ and $a_0(980)$ do not conform to standard $q\bar{q}$ quark model expectations. The biggest departures from theoretical predictions based on the $q\bar{q}$ model are in the total width (predicted Γ ~500 MeV, observed Γ ~50 MeV) and in the $\gamma\gamma$ coupling (predicted ~4.5 keV for f_0, ~1.5 keV for a_0, observed ≤0.6 keV for f_0, ~0.2 keV for a_0). Two alternative hypotheses (2) are presently under discussion for their nature: they could be a four quark state $q\bar{q}q\bar{q}$ (R~1 fm) (3) or a $K\bar{K}$ molecule (R~1.7 fm) (4). Different BR's are expected depending on their nature, as can be seen in Table 1 in the case of the f_0.

Recent studies using lattice QCD (5) suggest that $q\bar{q}q\bar{q}$ states occurs generically near meson-meson thresholds. The recent observation of $\phi \to f_0\gamma$, $\phi \to a_0\gamma$ with B.R. $\sim 10^{-4}$(6; 7) seems to be in favour of the $q\bar{q}q\bar{q}$ scenario. The observation from Crystal Barrel of an isoscalar $f_0(1365)$ (8) and an isovector $a_0(1450)$ (9) as members of the $^3P_0$ nonet allows us to search for an explanation for the $f_0(980)$, $a_0(980)$ outside the $q\bar{q}$ model.

1.1.2 The pseudoscalar sector: $\phi \to \eta\gamma$, $\phi \to \eta'\gamma$

The reason for studying ϕ radiative decays in η and η' is twofold since the measurement of BR($\phi \to \eta'\gamma$) can help in defining the gluonic content of the η' while the measurement of the ratio R=BR($\phi \to \eta'\gamma$)/ BR($\phi \to \eta\gamma$) can help in establishing the value of the $\eta - \eta'$ mixing angle θ_P.
The presence of gluon admixture in the η' wavefunction is a longstanding problem that could be solved by an accurate measurement of BR($\phi \to \eta'\gamma$): theoretical predictions range from as low as 10^{-6} in models with gluonium admixture (10) or with strong QCD violations (11) to 10^{-4} in different realizations of the quark model (12; 13; 14; 15). The recent measurement of BR($\phi \to \eta'\gamma$) by the CMD-2(16) and SND(17) collaboration at VEPP-2M seems to exclude a gluonium admixture.

The value of θ_P has been discussed many times in the last thirty years: the quadratic Gell Mann Okubo mass formula gives $\theta_P \sim -10^o$ while recent analyses, based mainly on decays $J/\psi \to VP$, give θ_P in the range from $-17^o to -20^o$. A crucial test, originally proposed by Rosner (14) is the measurement of the ratio R=BR($\phi \to \eta'\gamma$)/ BR($\phi \to \eta\gamma$). This ratio predicts 7.6×10^{-3} for $\theta_P \sim -20^o$ and 6.2×10^{-3} for $\theta_P \sim -16.9^o$.

1.2 $\phi \to \pi^+\pi^-\pi^0$

About 15% of the ϕ decay into $\pi^+\pi^-\pi^0$. These final states can be due to three different mechanisms (see fig.1):

1. $\phi \to \rho\pi$ decay where $\rho\pi$ include all the three possible charge states (namely $\rho^+\pi^-$, $\rho^0\pi^0$ and $\rho^-\pi^+$) with the same isospin weights;
2. $\phi \to \pi^+\pi^-\pi^0$ direct decay;
3. $e^+e^- \to \omega\pi^0$, with $\omega \to \pi^+\pi^-$.

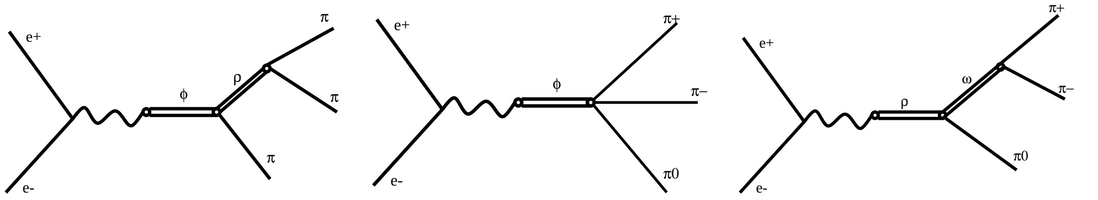

Figure 1: Feymnan diagrams contributing to the $\pi^+\pi^-\pi^0$ final state.

The fit of the Dalitz-plot distribution of this three-body decay allows us to discriminate between the three contributions. In particular it is possible to observe the direct contribution (number 2) as predicted by several theoretical models, that has never been observed in previous experiments. The only up to now published analysis of this kind (18) finds a Dalitz-plot fully dominated by the $\rho\pi$ contribution and only a limit of the direct decay to be below $\sim 10\%$.

Furthermore a precision measurement of the ρ line shape parameters is also possible. In particular the same amount of events corresponding to the three charge states of the ρ, allows us to make comparisons between ρ^+ and ρ^- (CPT test) and between charged ρ and ρ^0. A mass or width difference between $\rho^\pm$ and ρ^0 is a signature of isospin violation as observed in other meson and baryon isospin multiplets.

2 ϕ radiative decays

2.1 Selection criteria for radiative decays

Some steps of the analysis and some definitions are very similar for most of the processes studied in this paper.

All the processes under study are characterized by the presence of prompt photons, i.e. photons coming from the the I.P. These photons are detected as clusters in the calorimeter that obey the relation $t - r/c = 0$, where t is the arrival time on the calorimeter, r is the distance of the cluster from the I.P., and c is the speed of light. We define a photon to be "prompt" if $|t - r/c| < 5\sigma_t$, where we use as time resolution of the calorimeter the parameterization $\sigma_t = 110$ ps$/\sqrt{E(\mathrm{GeV})}$. This $t - r/c$ interval is often referred to as "time window" in the following sections. An acceptance angular region corresponding to the polar angle interval $21^o \div 159^o$ is defined for the prompt photons, in order to exclude the blind region around the beam-pipe.

Most of the analyses described in this paper make use of a constrained fit ensuring kinematic closure of the events. The free parameters of the fit are: the three coordinates (x, y, z) of the impact point on the calorimeter, the energy, and the time of flight for each photon coming from the I.P., the track curvature and the two angles ϕ and θ for each charged pion also coming from the I.P., the two energies of the beams, and the three coordinates of the position of the I.P. The analysis procedure adopted is the following:

1. events with the appropriate number of prompt photons and charged tracks are selected from the "radiative stream";
2. the kinematic fit is applied on these events a first time with the constraints of the total energy and momentum conservation and satisfying $t - r/c = 0$ for each prompt photon;
3. other selection criteria are applied to separate the signal from background;
4. the kinematic fit is applied a second time on the surviving events with the same constraints as before plus other ones imposing the invariant masses of the particles present in the intermediate states (π^0's, η's etc.).

2.2 Luminosity measurement

Knowledge of the integrated luminosity is necessary for the measurement of the cross-sections like $\sigma(e^+e^- \to \phi \to \eta\gamma \to \gamma\gamma\gamma)$, $\sigma(e^+e^- \to \omega\pi^0 \to \pi^0\pi^0\gamma)$ and $\sigma_{hadronic}$.

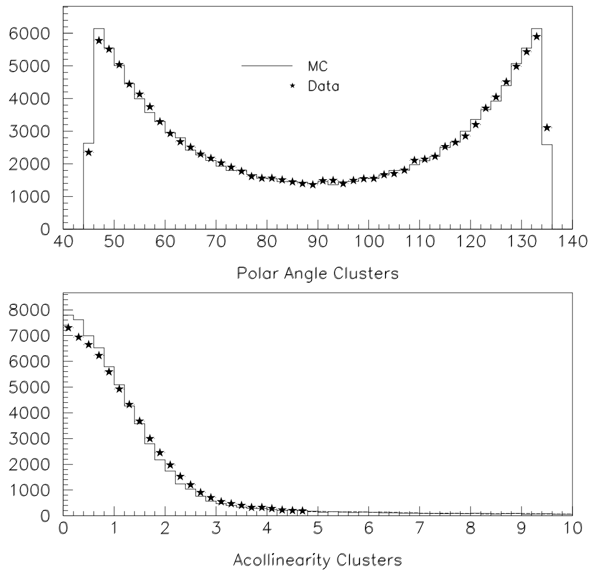

Figure 2: Comparison between data and MC of polar angle and acollinearity for Bhabha events.

The integrated luminosity has been measured with large angle Bhabha scattering events using only the calorimeter information. The measurement is described in detail in ref.(19). The absolute error on the luminosity measurement can be estimated in $\leq 3\%$. Fig.2 shows a comparison between data and Monte Carlo for polar angle and acollinearity of large angle Bhabha electrons and positrons, that are the relevant quantities for the evaluation of the luminosity. The agreement between the distributions is good.

2.3 $\phi \to f_0\gamma$, with $f_0 \to \pi^+\pi^-$

The analysis of the $\phi \to f_0\gamma$ decay in the charged channel $f_0 \to \pi^+\pi^-$ has been performed on a sample of 1.8 pb^{-1} of collected data by looking at the spectrum of the production cross section of $\pi\pi\gamma$ events as a function of $\pi^+\pi^-$ invariant mass squared, Q^2(20). Two other processes contribute to the $\pi^+\pi^-\gamma$ final state: *Initial State Radiation* (ISR), in which the photon is emitted by the incoming electron or positron, and *Final State Radiation* (FSR), in which the γ is emitted by one of the two pions. The latter process gives rise to an interference with the signal whose sign is not known.

The $\pi^+\pi^-\gamma$ events are selected using both drift chamber and electromagnetic calorimeter informations. The first step of the signal selection requires a *prompt* neutral cluster and a vertex close to the interaction point. This general selection identifies not only $\pi^+\pi^-\gamma$ events, but also $\mu^+\mu^-\gamma$ events and a huge amount of radiative Bhabhas.
The kinematical properties alone are not enough to suppress the $ee\gamma$ events, therefore a likelihood method has been developed which uses both the particle time of flight and some informations coming from the cluster associated to the particle. This method has a 95% selection efficiency for a pion and a $\sim$ 94% rejection power for electrons.

After the likelihood selection, kinematical cuts have been chosen in order to get a further reduction of $\mu^+\mu^-\gamma$ and $e^+e^-\gamma$ background and to emphasize the $\phi \to \pi^+\pi^-\gamma$ decay contribution. For both these purposes particles have been selected in the central part of the detector ($45^o < \theta < 135^o$), since the polar angle distribution of the charged tracks from $e^+e^-\gamma$ and $\mu^+\mu^-\gamma$ events and of the photon from ISR are enhanced at small angles.

The last cut selects events based on the invariant mass of the charged track identified by applying 4-momentum conservation in the hypothesis of a massless neutral particle:

$$(\vec{p}_1 + \vec{p}_2)^2 - \left(M_\phi - \sqrt{\vec{p}_1^2 + M_{TR}^2} - \sqrt{\vec{p}_2^2 + M_{TR}^2}\right)^2 = 0$$

where $\vec{p}_1$ and $\vec{p}_2$ are the tracks momenta and M_{TR} is the track mass, assumed to be the same for both charged particles. The distribution of the variable M_{TR} before and after the likelihood cut is shown in fig.3. The pion peak is clearly visible and the signal events are selected in a window of $\pm$10 MeV around M_π = 140 MeV, the central value of the fit.

In order to compare the experimental results with the theoretical predictions for $e^+e^- \to \pi^+\pi^-\gamma$ process, the Q^2 spectrum has been corrected by the total selection efficiency as a function of Q^2, represented in fig. 4. The low efficiency at high Q^2 values is due to the trigger *cosmic veto*, which can mistakes a $\pi^+\pi^-\gamma$ event with a soft photon for a cosmic event.
At low Q^2 values the efficiency decreases because of the cuts applied to reduce $\pi^+\pi^-\pi^0$ background.

Owing to the high rate of $\phi \to \pi^+\pi^-\pi^0$ decays, $\pi^+\pi^-\pi^0$ background can survive $\pi^+\pi^-\gamma$ selection: the contamination is higher at low Q^2 values, and it has been evaluated by fitting the track mass distribution of events identified as $\pi^+\pi^-\pi^0$ for each Q^2 bin and extrapolating the fit function in the $\pi^+\pi^-\gamma$ mass region.

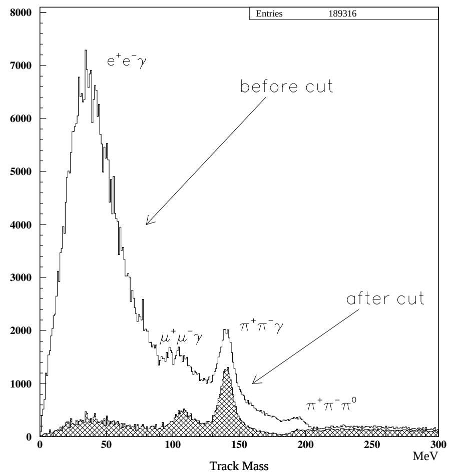

Figure 3: Distribution of the variable M_{TR} (see text) before and after the likelihood selection. The pion and muon peaks are clearly visible.

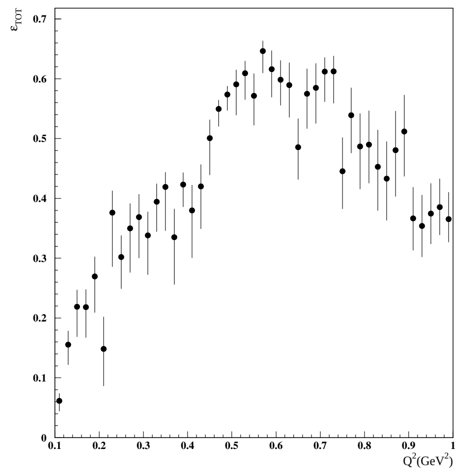

Figure 4: Total selection efficiency for a $\pi^+\pi^-\gamma$ event in the central part of the detector; the trigger cosmic veto determines the low efficiency at high Q^2 values, while the low Q^2 inefficiency is due to the kinematical cuts applied to reduce $\pi^+\pi^-\pi^0$ background.

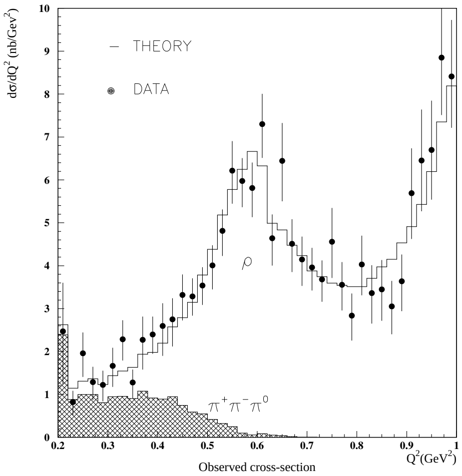

Figure 5: Experimental cross-section as a function of Q^2 compared to the theoretical one for pure QED contributions.

The experimental data, corrected by the total efficiency, have been fitted using the theoretical spectrum including ISR and FSR contributions only. The fit parameters are the integrated luminosity and the normalization factor of $\pi^+\pi^-\pi^0$ spectrum with respect to $\pi^+\pi^-\gamma$ one. In fact to evaluate the $\pi^+\pi^-\pi^0$ background contribution to the experimental differential cross-section, for $\pi^+\pi^-\pi^0$ events has been assumed the same selection efficiency as for $\pi^+\pi^-\gamma$ ones, the latter fit parameter (Norm) takes into account possible differences in the overall efficiency.

The results of the fit are: $L = 1774\,\mathrm{nb}^{-1}$, Norm $= 1.16$, with a $\chi^2/ndf = 33/45$. Fig.5 shows the comparison of the experimental differential cross-section for the $e^+e^- \to \pi^+\pi^-\gamma$ process with the theoretical one. The comparison is good and no f_0 signal is needed, with the available statistics, to describe the spectrum. An upper limit on the branching ratio for the decay $\phi \to f_0\gamma \to \pi^+\pi^-\gamma$ can be set by fitting the Q^2 spectrum in the region $Q^2 < 0.84\,\mathrm{GeV}^2$ and extrapolating it in the photon energy range $20\,\mathrm{MeV} < E_\gamma < 120\,\mathrm{MeV}$, where the signal is expected. An excess of 35 ± 160 events, with respect to the ones predicted by pure QED, is found. Assuming the isospin symmetry and ignoring the interference with FSR, this number corresponds to an upper limit on the value of the branching ratio of:

$$\mathrm{BR}(\phi \to f_0\gamma \to \pi^+\pi^-\gamma) < 1.64 \times 10^{-4} \quad @\ 90\%\ \mathrm{C.L.}\ .$$

2.4 $\phi \to \eta\pi^0\gamma$ with $\eta \to \gamma\gamma$

This process is characterized by 5 prompt photons without charged tracks in the final state. It is expected to be dominated by the $\phi \to a_0\gamma$ decay, in which the $a_0(980)$ decays into $\eta\pi^0$. The spectrum of the photon radiated by the ϕ is expected to be broad and peaked at ~ 50 MeV. Two other processes contribute to this final state: $\phi \to \rho^0\pi^0$ and the non-resonant process $e^+e^- \to \omega\pi^0$ with the rare decays of ρ^0 and ω into $\eta\gamma$.

The main background comes from $\pi^0\pi^0\gamma$ final state, which is dominant in the 5 photon sample; the expected number of events is 10 times bigger than the signal. The other relevant background comes from the $\phi \to \eta\gamma$ decay, with 3 and 7 photons in the final state, that can be reconstructed as 5 photon events due to accidentals in the calorimeter or photon splittings and mergings. According to the MC the probability for both processes to be reconstructed as 5 photon events is about 3%, then due to their high branching ratio the expected number of events in the 5 photon sample is also of the order of 10 times the signal.

The events are selected by requiring:

1. no tracks in the drift chamber,
2. total energy in the calorimeter greater than 900 MeV,
3. exactly 5 prompt photons in the angular acceptance region.

On the 2200 events selected in the 2.4 pb^{-1} sample, a first kinematic fit has been applied by imposing constraints on the total energy and momentum conservation, and on the consistency of time and position in the calorimeter ($t - r/c = 0$) for each photon. A cut corresponding to $P(\chi^2) < 1\%$ has been applied.

Then for each event three different variables are constructed in order to test the three hypotheses:

1. $\eta\pi^0\gamma$ hypothesis: $D_{\eta\pi^0\gamma} = \sqrt{\frac{(M_{12}-M_{\pi^0})^2}{\sigma^2_{\pi^0}} + \frac{(M_{34}-M_\eta)^2}{\sigma^2_\eta}}$
2. $\pi^0\pi^0\gamma$ hypothesis: $D_{\pi^0\pi^0\gamma} = \sqrt{\frac{(M_{12}-M_{\pi^0})^2}{\sigma^2_{\pi^0}} + \frac{(M_{34}-M_{\pi^0})^2}{\sigma^2_{\pi^0}}}$
3. $\eta\gamma$ hypothesis: $D_{\eta\gamma} = \sqrt{\frac{(M_{12}-M_\eta)^2}{\sigma^2_\eta} + \frac{(E_3-E_{rad})^2}{\sigma^2_{rad}}}$

The value of each D-variable is obtained by choosing the photon pairing that minimizes it. M_{12} and M_{34} are the invariant masses of the photon pairs, E_{rad}=363 MeV. $\sigma_\eta = 20$ MeV and $\sigma_{\pi^0} = 9$ MeV have been evaluated from the data themselves, by fitting the invariant masses distribution on a sample of events. σ_{rad} is obtained from the energy resolution of the calorimeter.

The following cuts are applied:

1. $D_{\eta\pi^0\gamma} < D_{\pi^0\pi^0\gamma}$ in order to select the events that have a bigger probability to be $\eta\pi^0\gamma$ rather than $\pi^0\pi^0\gamma$ (see fig.6)
2. $D_{\eta\gamma} > 2$; in fig.7 is shown that this cut is able to reject events in the peak of E_{rad} at 363 MeV, that correspond to the η mass peak.

On the 240 events selected a second kinematic fit is applied, imposing as further constraints the two invariant masses of η and π^0; a cut corresponding to $P(\chi^2) < 1\%$ has been applied, and the 153 surviving events form the final sample.

The efficiencies for signal and backgrounds have been evaluated by MC, taking into account the dependence on photon energy. The resulting efficiencies are listed in Tab.2: in the first column is reported the trigger plus the background filter one; in the second column, the efficiency of the 5 prompt photon cut, that is mostly due to the angular cut at 21^o, and in third one is reported the effect of the selection and of the two kinematic fits.

In fig.8 are reported the spectrum of the radiated photon, and the invariant mass spectrum of all the other 4 ones (the invariant mass of the $\eta\pi^0$ system). These spectra are corrected for the dependence of

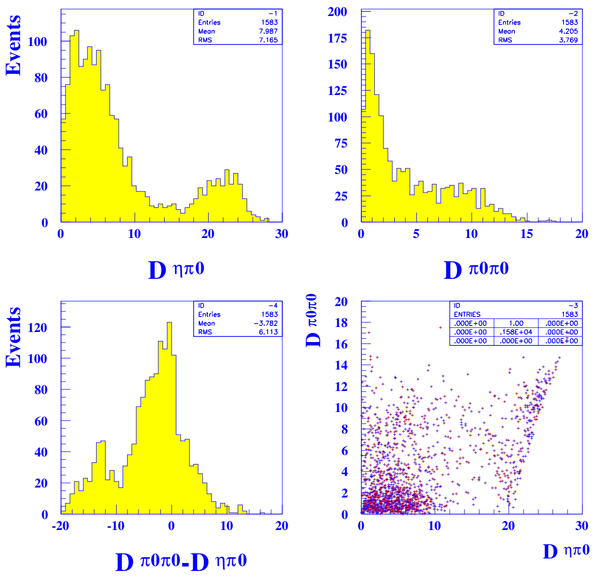

Figure 6: D-variables for the $\eta\pi^0\gamma$ and $\pi^0\pi^0\gamma$ hypotheses; a cut is applied on their difference by selecting the positive part of the distribution.

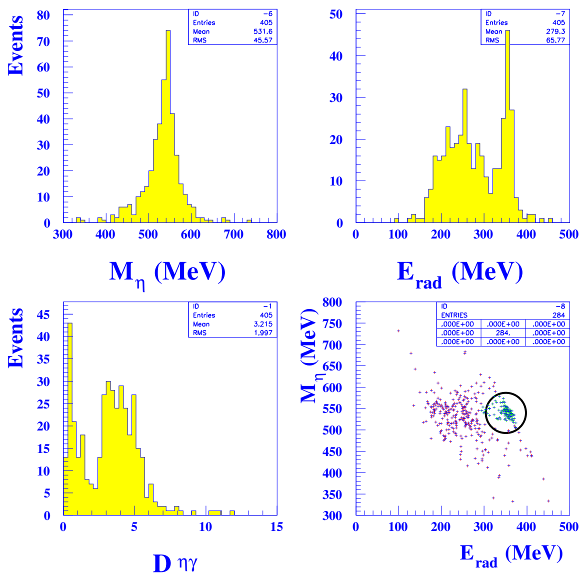

Figure 7: Rejection of $\eta\gamma$ background, the circle in the scatter plot shows the rejected region with the cut $D_{\eta\gamma} > 2$.

Process	Trigger + filters	5 prompt photons	Selection + kin. fits	Total
$\phi \to a_0\gamma \to \eta\pi^0\gamma$	0.81	0.70	0.42	0.24
$\phi \to \rho^0\pi^0 \to \eta\pi^0\gamma$	0.77	0.70	0.31	0.17
$\phi \to f_0\gamma \to \pi^0\pi^0\gamma$	0.80	0.70	$4.5{\cdot}10^{-3}$	$2.5{\cdot}10^{-3}$
$\phi \to \rho^0\pi^0 \to \pi^0\pi^0\gamma$	0.80	0.70	0.04	0.02
$e^+e^- \to \omega\pi^0 \to \pi^0\pi^0\gamma$	0.82	0.70	0.04	0.02
$\phi \to \eta\gamma \to 3\gamma$	0.78	0.03	-	$< 5 \cdot 10^{-4}$
$\phi \to \eta\gamma \to 7\gamma$	0.80	0.03	0.05	10^{-3}

Table 2: Efficiencies evaluated by means of the MC simulation; for the $e^+e^- \to \omega\pi^0 \to \eta\pi^0\gamma$ process we assume the same efficiencies of the $\pi^0\pi^0\gamma$ final state.

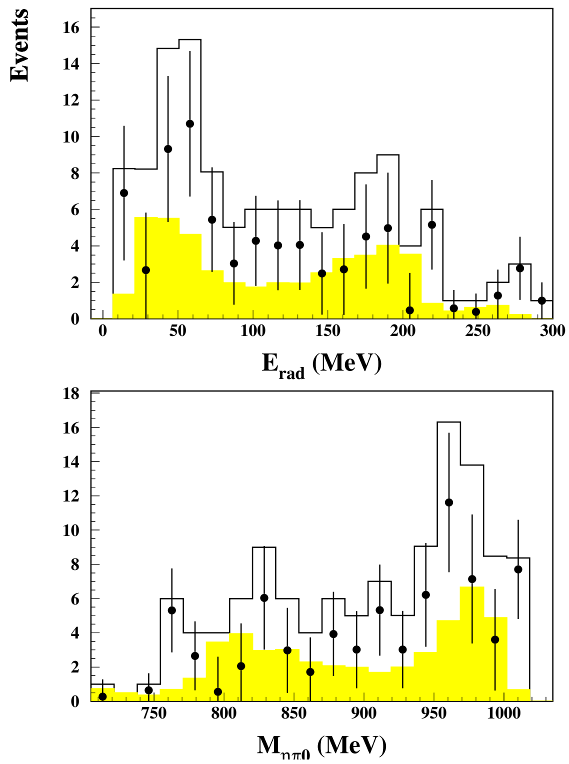

Figure 8: Upper: energy of the "radiated" photon; lower: invariant mass of the $\eta\pi^0$ system. Full histograms: data; shadowed ones: expected background (from MC); black points: data - background difference.

photon detection efficiency on energy. The background spectra, superimposed in fig.8, are predictions obtained by MC by weighting the background processes with the product of their expected branching ratio times their efficiency.

In order to evaluate the $Br(\phi \to \eta\pi^0\gamma)$ we consider the whole spectrum: 118$\pm$ 11 events are selected (N), with an expected background of 47$\pm$ 7 (B), and assuming $Br(\eta \to \gamma\gamma) = 39.2\%$

$$Br(\phi \to \eta\pi^0\gamma) = \frac{N - B}{\varepsilon L \sigma_\phi Br(\eta \to \gamma\gamma)} = (0.98 \pm 0.18_{stat}) \cdot 10^{-4} \quad (1)$$

where $L = 2.4$ pb^{-1}, and $\sigma_\phi = 3.2$ μb. The systematic uncertainty on this measurement is still under study.

This value is in agreement within the errors with the results of the Novosibirsk experiments(7; 6).

2.5 $\phi \to \eta\gamma$, with $\eta \to \gamma\gamma$

The $\phi \to \eta\gamma \to \gamma\gamma\gamma$ decay, having an higher BR (0.49%) and an harder energy spectrum with respect to the rest of ϕ radiative decays, is a good calibration sample for multi–photon final states. It is also used to evaluate the ϕ cross section and to normalize BRs of rarer decays.

Since the energy of the radiative photon ($E_{\gamma_{\rm rad}} \sim 360$ MeV) is inside the energy range of the γ's coming from the η ($150 < E_{\gamma_\eta} < 500$ MeV), the kinematic fit is used to select the $\gamma\gamma$ pair assigned to the meson. For each event with three photons in time window the fit is applied in the $\eta\gamma$ hypothesis using the η mass constraint for the three possible photons' combination. The minimum χ^2 is then selected.

The only relevant background for this channel comes from the $\phi \to \pi^0\gamma$ decay (S/B $\sim$ 4). Since the energy of the primary photon ($E_{\gamma_{\rm rad}} \sim 500$ MeV) is higher than the one of the signal, the fit can reconstruct it as an $\eta\gamma$ event by wrongly combining the radiative photon with a γ coming from the π^0 ($E_{\gamma_{\pi^0}} < 500$ MeV). Being the third photon constrained in the 360 MeV region, the three photons are monochromatic for $\pi^0\gamma$ events after the fit. The background is therefore rejected using the ΔE variable, energy difference of the $\gamma\gamma$ pair, requiring $|\Delta E| < 330$ MeV: as it is shown in Fig. 9.up-left, $\pi^0\gamma$ events are peaked at high $|\Delta E|$ values while signal has a flat distribution.

A sample corresponding to 1.84 pb^{-1} have been analysed: among 226736 events with at least 3 clusters, 183345 satisfy angular acceptance cut and 45889 have also 3 photons in time window with $E > 20$ MeV. After the χ^2 cut and the background rejection the sample is reduced to 18504 events. The resulting angular and energy distributions of the radiative photon, together with the $\gamma\gamma$ pair invariant mass, are shown in Fig. 9. All distributions are well in agreement with Monte Carlo expectations. The resulting η mass is within 0.2% the expected value.

In order to check if $\gamma\gamma\gamma$ QED background can simulate the signal, angular distributions between photons' pairs have been studied (Fig. 10). The excellent agreement with $\eta\gamma$ simulated events leaves no room for any residual background.

The ϕ visible cross section has been evaluated by measuring

$$\sigma(e^+e^- \to \phi \to \eta\gamma \to \gamma\gamma\gamma) = \frac{N_{\eta\gamma}}{L \times \varepsilon_{\rm ana}} \cdot \frac{1}{{\rm BR}(\phi \to \eta\gamma \to \gamma\gamma\gamma)} \quad (2)$$

and using ${\rm BR}(\phi \to \eta\gamma \to \gamma\gamma\gamma) = (0.49 \pm 0.02)\%$. Luminosity is estimated by using large angle Bhabha's ($\theta > 45°$) while analysis efficiencies, listed in Tab. 3, are evaluated from Monte Carlo.

We quote:

$$\sigma_\phi = (\,3.19 \pm 0.02\,({\rm stat.}) \pm 0.26\,({\rm syst.})\,)\ \mu{\rm b} \quad (3)$$

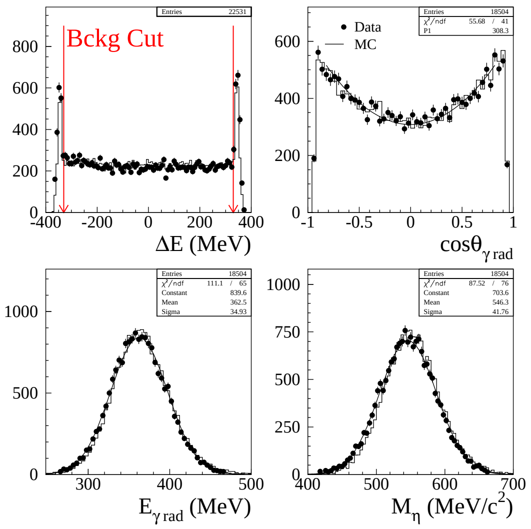

Figure 9: Comparison between data (—) and Monte Carlo (•) distributions for $\phi \to \eta\gamma \to \gamma\gamma\gamma$ events: energy difference of the two photons assigned to η (up-left) – the two peaks are due to the $\phi \to \pi^0\gamma$ background; angular distribution (up-right) and energy spectrum (down-left) of the radiative photon; $\gamma\gamma$ pair invariant mass (down-right). Last two variables are obtained after photons' assignment from the fit but using energies reconstructed without constraints.

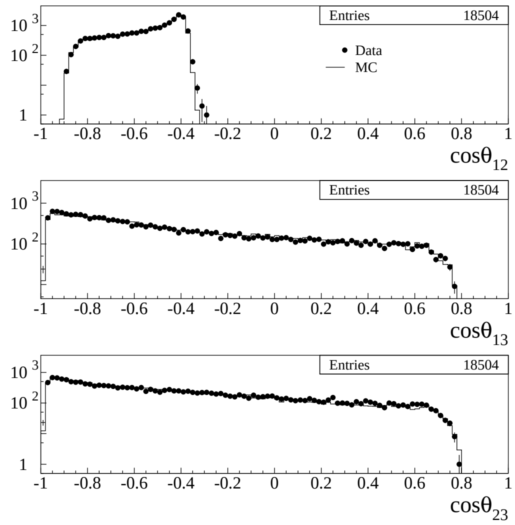

Figure 10: Opening angles between photons' pairs of $\phi \to \eta\gamma \to \gamma\gamma\gamma$ events for data and Monte Carlo. Photons named 1 and 2 are the ones assigned to η.

Table 3: Analysis efficiencies for $\phi \to \eta\gamma \to \gamma\gamma\gamma$ events.

Efficiency	Contribution
$\varepsilon_{\rm cl} = 76.0\%$	Trigger, background rejection and event classification
$\varepsilon_{\rm sel} = 93.7\%$	Acceptance and time window cuts
$\varepsilon_{\chi^2} = 98.5\%$	χ^2 cut
$\varepsilon_{\Delta E} = 91.3\%$	ΔE cut
$\varepsilon_{\rm ana} = 64.3\%$	Total

Table 4: Error contributions to ϕ cross section measurement using $\phi \to \eta\gamma \to \gamma\gamma\gamma$ events.

VARIABLE	VALUE	METHOD
$\mathrm{BR}_{\gamma\gamma\gamma}$	4%	From PDG
L	5%	Comparing trigger vs L3 vs offline values
$\varepsilon_{\rm cl}$	5%	Conservative estimate using a small data control sample without event classification
$\varepsilon_{\rm sel}$	1.0%	Fit to $\cos\theta_{\gamma\,\rm rad}$ distribution in different angular regions for acceptance. No contributions from TW cut ($\mathrm{TW}_{\rm max}$ $2 \to 3$ ns: no changes) and clustering ($\varepsilon_{\rm MC} = 99.9\%$)
ε_{χ^2}	0.6%	50% of the wrong assignments percentage as obtained from MC
$\varepsilon_{\Delta E}$	0.3%	Comparison between loss of events counted with MC and the estimate on data fitting the $\vert\Delta E\vert < 300$ MeV region

This value is in good agreement with CMD-2 result, obtained using $K_S \to \pi^+\pi^-$ events: $\sigma_\phi = (3.114 \pm 0.034 \pm 0.048)$ μb(21).

Complete evaluation of systematics is in progress. At the moment a preliminary estimate of the contributions is summarized in Tab. 4.

In addition to the analysis described above an alternative method has been developed for measuring the ratio $\mathrm{Br}(\phi \to \eta\gamma)/\mathrm{Br}(\phi \to \pi^0\gamma)$ without using any kinematic fit(22).

2.6 The ratio $\mathbf{BR}(\phi \to \eta'\gamma)/\mathbf{BR}(\phi \to \eta\gamma)$

Two different decay chains giving rise to both fully neutral and charged/neutral final states have been used to study the ratio $R_\phi = BR(\phi \to \eta'\gamma)/BR(\phi \to \eta\gamma)$:

1. $\phi \to \eta'\gamma \to \eta\pi^+\pi^-\gamma \to \pi^+\pi^-\gamma\gamma\gamma$
2. $\phi \to \eta'\gamma \to \eta\pi^0\pi^0\gamma \to 7\gamma$

A very clean control sample is given by $\phi \to \eta\gamma$ decays with identical final state:

1. $\phi \to \eta\gamma \to \pi^+\pi^-\pi^0\gamma \to \pi^+\pi^-\gamma\gamma\gamma$

2. $\phi \to \eta\gamma \to \pi^0\,\pi^0\,\pi^0\,\gamma \to 7\gamma$

These events, being 2-3 order of magnitude more probable than the corresponding $\phi \to \eta'\gamma$ ones, constitute also the main source of background for their detection. For this reason a kinematic fit with mass constraints is needed to obtain a satisfactory signal to background ratio in these final states.

Since the final state is identical for the $\phi \to \eta'\gamma$ and $\phi \to \eta\gamma$ corresponding channel, most of the systematics will cancel if we evaluate the ratio R_ϕ using the same final state to count $\phi \to \eta\gamma$ and $\phi \to \eta'\gamma$ events.

2.6.1 $\pi^+\pi^-\gamma\,\gamma\,\gamma$ final state

For $\phi \to \eta'\gamma$ events this final state is characterized by a nearly monochromatic photon with $E_\gamma = 60\,\mathrm{MeV}$ recoiling against the η', and two (harder) photons coming from $\eta \to \gamma\gamma$ annihilation. On the contrary, for $\phi \to \eta\gamma$ events the radiative photon, still monochromatic, is the most energetic one, with $E_\gamma = 363\,\mathrm{MeV}$ and the two (softer) other photons come from $\pi^0 \to \gamma\gamma$ annihilation.

In addition to the $\phi \to \eta\gamma$ background, some background events can be expected from $\phi \to K_S\,K_L$ events with one charged and one neutral vertex where at least one photon is lost and the K_L is decaying near the interaction point and from $\phi \to \pi^+\pi^-\pi^0$ events with an additional cluster counted.

A first level *topological* selection runs as follows:

- 3 and only 3 prompt neutral clusters (as described above) with $E_\gamma > 10\,\mathrm{MeV}$ and $21° < \theta_\gamma < 159°$
- 1 charged vertex inside the cylindrical region $r < 4$cm; $|z| < 8$cm

and is common for both $\phi \to \eta'\gamma$ and $\phi \to \eta\gamma$ events.

Background from $\pi^+\pi^-\pi^0$ events is strongly reduced by means of a cut on the sum of the energies of the charged tracks assumed to be pions: it is expected larger for three pions events than for radiative events.

Background from $\phi \to K_S\,K_L$ is reduced for $\phi \to \eta\gamma$ using the fact that the spectrum for photons coming from kaons is limited to energies below 280 MeV while in $\phi \to \eta\gamma$ we expect at least one photon with energy exceeding 300 MeV.

The same cut cannot be applied to $\phi \to \eta'\gamma$ events where the energy spectrum of photons is different: in this case however, a suitable variable to select the signal has been found to be the sum of the energies of the three photons $E_{\gamma\gamma\gamma}$. In conclusion one applies the cuts:

- For $\phi \to \eta\gamma$ selection:
  - $E_{\pi^+} + E_{\pi^-} < 550\,\mathrm{MeV}$ ($\varepsilon_{3\pi} \simeq 1.5 \cdot 10^{-3}$)
  - $E_\gamma^{\max} > 300\,\mathrm{MeV}$ ($\varepsilon_{K_L\,K_S} \simeq 2 \cdot 10^{-4}$)
- For $\phi \to \eta'\gamma$ selection:
  - $E_{\pi^+} + E_{\pi^-} < 412\,\mathrm{MeV}$ ($\varepsilon_{3\pi} \simeq 1 \cdot 10^{-4}$)
  - $E_{\gamma\gamma\gamma} > 520\,\mathrm{MeV}$ ($\varepsilon_{K_L\,K_S} \simeq 1 \cdot 10^{-4}$)

The efficiency for this selection is evaluated from Monte Carlo to be 39.6% for $\phi \to \eta'\gamma$ and 37.9% for $\phi \to \eta\gamma$ events.

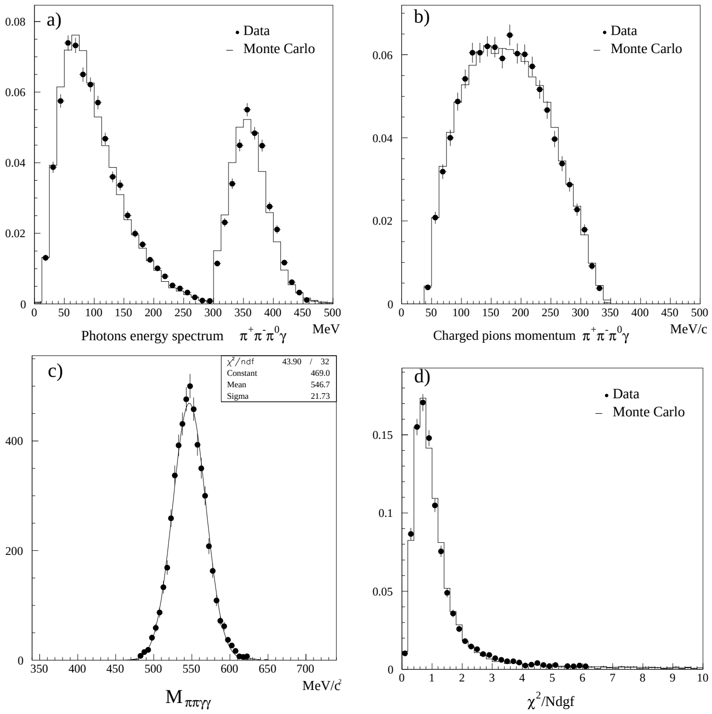

Figure 11: Monte Carlo (pure $\phi \to \eta\gamma$) versus data for $\pi^+\pi^-\gamma\,\gamma\,\gamma$ events: a) Cluster energy spectrum; b) Charged pions momentum spectrum; c) η invariant mass distribution; d) χ^2 of kinematic fit

Contamination from $\phi \to \eta\gamma$ events into the $\phi \to \eta'\gamma$ sample is at this level still very high (S/B $\sim 10^{-3}$): thus a kinematic fit with mass constraints (see section 2.1) has been implemented for both the decay chain hypotheses constraining all intermediate masses. The energy spectrum of the photons gives no problem in assigning clusters to particle originating them: as already noticed above radiative photon is the most energetic one in $\phi \to \eta\gamma$ events, while it is the less energetic one in $\phi \to \eta'\gamma$ events; the other two cluster belong to π^0 and η respectively in the two cases. A cross cut on $\mathcal{P}(\chi^2_{\eta'\gamma}) > 25\%$ *and* $\mathcal{P}(\chi^2_{\eta\gamma}) < 1\%$ has proven by Monte Carlo to maximize the significance $S/\sqrt{B}$ and has thus been chosen as final selection criterium for $\phi \to \eta'\gamma$ events. Final Monte Carlo efficiency after this cut is 18.6% for $\phi \to \eta'\gamma$ while for $\phi \to \eta\gamma$ a 90% C.L. upper limit can be set to $4.4 \cdot 10^{-5}$ giving rise to an expected S/B ratio > 35 (90% C.L.) if one uses the PDG'98 value for BR($\phi \to \eta'\gamma$).

A selection cut can also be put to select $\phi \to \eta\gamma$ events, and has been chosen in a very conservative way to be $\mathcal{P}(\chi^2_{\eta\gamma}) > 1\%$ due to the low background on this channel. With this cut one has a final efficiency of 31.9% for $\phi \to \eta\gamma$ and selects a very pure set of events with background (estimated from Monte Carlo, and confirmed by a fit to the η mass peak) being $\sim 0.1\%$ of the sample.

The abundant and pure $\phi \to \eta\gamma$ events can be used as control sample for systematic effects on the efficiency, and to compare data versus Monte Carlo distributions for the variable on which the cuts are set.

All comparisons (see fig.11) show very good agreement (within 1-2%) between data and Monte Carlo, and since the dependence of the efficiency on the cuts is not critical (for example moving the cut on the charged pions energy by $\pm 1\%$ changes $\phi \to \eta\gamma$ selection efficiency by $\sim 0.1\%$, for a more detailed

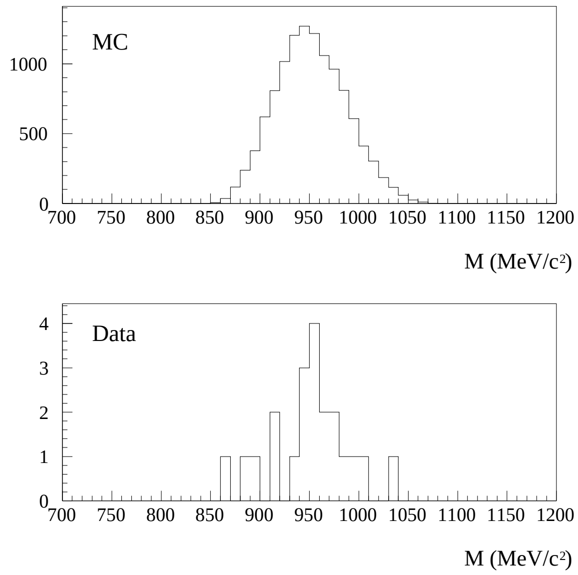

Figure 12: Invariant mass of two charged tracks and two most energetic photons for events selected as $\phi \to \eta'\gamma$. Data (lower plot) is compared to pure monte Carlo $\phi \to \eta'\gamma$ events.

discussion see (23)) the overall systematic error on the estimation of efficiencies is very small. Also, when evaluating the ratio R_ϕ most of the systematics will cancel out due to the strong similarities between the two categories of events. With the statistics of $\sim 2.4\,\mathrm{pb}^{-1}$ of 1999 run we found 21$\pm$ 4.6 $\phi \to \eta'\gamma$ events in this decay chain with less than one event of background expected at 90% C.L., while with the $\phi \to \eta\gamma$ selection selects 6696 events in the same runs. The distribution of the invariant mass of the two charged pions and the two most energetic photons in the event is shown in fig. 12 compared to the Monte Carlo expected for pure $\phi \to \eta'\gamma$ events. Solving for R_ϕ we get:

$$R_\phi = \frac{N_{\eta'\gamma}}{N_{\eta\gamma}} \frac{\varepsilon_{\eta\gamma}}{\varepsilon_{\eta'\gamma}} \frac{BR(\eta \to \pi^+\pi^-\pi^0)BR(\pi^0 \to \gamma\gamma)}{BR(\eta' \to \pi^+\pi^-\eta)BR(\eta \to \gamma\gamma)}$$

and, thus:

$$R_\phi = (7.1 \pm 1.6(\mathrm{stat.}) \pm 0.3(\mathrm{syst.})) \cdot 10^{-3}$$

where the systematic error is dominated by the uncertainty on the value of the intermediate branching ratios (4%). In fact systematic effects on luminosity evaluation and σ_ϕ cancel out exactly in the ratio, while trigger efficiency, streaming efficiency and reconstruction effects cancel almost exactly. This result on R_ϕ leads in turn to:

$$BR(\phi \to \eta'\gamma) = (8.9 \pm 2(\mathrm{stat.}) \pm 0.6(\mathrm{syst.})) \cdot 10^{-5}$$

This result has to be compared to the most recent results by CMD-2 and SND, which use the same final state(25; 26)

2.6.2 7γ final state

The high hermeticity of the KLOE EmC allows us to detect with high efficiency multiphoton final states. The $\phi \to \eta'\gamma \to \pi^0\pi^0\eta\gamma \to 7\gamma$ and its background $\phi \to \eta\gamma \to \pi^0\pi^0\pi^0\gamma \to 7\gamma$ are two such states, and

can be selected by seeking seven prompt clusters in the EmC with no charged track in the event.
As far as other backgrounds are concerned, only fully neutral channels are relevant. However, due to high hermeticity of the EmC, the most relevant of them, the $\phi \to K_S\,K_L \to 5\pi^0 \;\to 10\gamma$, may mimic a 7γ final state only in a very small fraction of events. Moreover, the prompt γ selection rules out all events where K_L is not decaying very near the beam pipe. A sample of $5 \cdot 10^5$ Monte Carlo events has been generated for this background, and no event survived the topological selection cuts. The simple, topological selection is common to both $\phi \to \eta\gamma$ and $\phi \to \eta'\gamma$ events and requires:

- 7 prompt neutral clusters with $21° < \theta < 159°$.
- No charged tracks.
- $|E_{tot} - 1020\,\mathrm{MeV}| < 130\,\mathrm{MeV}$

where E_{tot} is the sum of the energies of the selected clusters.
The efficiency of this cut is 30%. Events passing this cut are further analyzed in both hypotheses of being $\phi \to \eta\gamma$ and $\phi \to \eta'\gamma$ events.

To completely rule out any $\phi \to K_S\,K_L$ background a cut on $E_\gamma^{\max} > 300\,\mathrm{MeV}$ can be put for $\phi \to \eta\gamma$ events with essentially no loss in efficiency. Monte Carlo simulations, and fit to the η mass peak, show that background in the $\phi \to \eta\gamma$ channel is then again at the level of 0.1%.

No attempt is made to solve the combinatorial for the three π^0 's coming from the η decay, and the only identified photon is the radiative one, which is, as usual in $\phi \to \eta\gamma$, the most energetic photon of the event.

For $\phi \to \eta'\gamma$ the further analysis is based on a two-steps kinematic fit. First, a kinematic with no mass constraints is performed to achieve a better determination of the photons energies. Then a pairing procedure is applied in order to obtain the correct identification of the photons.

The starting point of this procedure is the observation that the most energetic photon of the event comes always from the η decay. The remaining six photons are then scanned to check the best pairing giving the correct η mass. Once the second photon is assigned to the η , the most energetic of the five remainders is coming from one of the π^0 's : Monte Carlo shows that in this way the first three photons are correctly assigned in 99.3% of the cases.

The remaining 4 photons give rise to twelve possible combinations: a χ^2-like function is built for each combination to compare the obtained masses to the expected ones, and among these the best five combinations are selected : in 96% of cases among these there is the correct one. Finally the five best combinations are fitted with a full constrained kinematic fit, where the π^0 's , η and η' invariant masses constraints are added to the constraints used in the preliminary fit. The combination minimizing the final χ^2 is then chosen to be the correct one, and the χ^2 of this fit is used as a discriminating variable for background suppression.

The combination found is the correct one in 90% of the cases, the main sources of mistakes being the radiative γ associated incorrectly to a π^0 (5%) and/or the 4 γ 's of the π^0 's being mismatched (5%).

The χ^2 corresponding to the best combination is compared to the one of a kinematic fit performed in the $\phi \to \eta\gamma$ hypothesis, with only the η mass as intermediate mass constraint. Using Monte Carlo events an optimized cut has been chosen in a triangular shaped region in the plane $\mathcal{P}(\chi^2_{\eta'\gamma}) - \mathcal{P}(\chi^2_{\eta\gamma})$. Analytically it can be described by the formula:

$$\mathcal{P}(\chi^2_{\eta'\gamma}) > 15\% + 3.4 \cdot \mathcal{P}(\chi^2_{\eta\gamma})$$

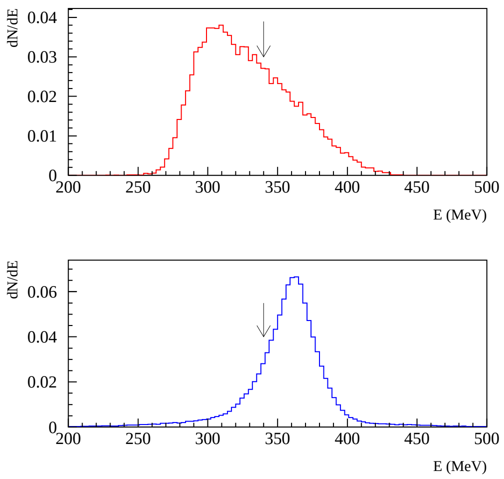

Figure 13: Monte Carlo energy spectrum of the most energetic cluster for events passing both $\phi \to \eta\gamma$ and $\phi \to \eta'\gamma$ event selection, and after the kinematic fit with no mass constraints. The plot shows $\phi \to \eta\gamma$ events (lower plot), $\phi \to \eta'\gamma$ events (upper plot) and the position of the selection cut (arrow).

This cut alone, although being able to reduce drastically the $\phi \to \eta\gamma$ background, is not enough to obtain a satisfactory Signal/Background ratio: indeed 5×10^{-4} $\phi \to \eta\gamma$ events still survive the cut against 15.6% of $\phi \to \eta'\gamma$, giving a S/B ratio of ≈ 0.8.
For this reason a further selection cut has been introduced.
The distribution of the energy of the most energetic photon after the kinematic fit is shown in fig. 13 for $\phi \to \eta'\gamma$ and $\phi \to \eta\gamma$ fully neutral events. A cut on this energy is able to scale down definitively the $\phi \to \eta\gamma$ background, even if it causes a somewhat loss in efficiency for the $\phi \to \eta'\gamma$ signal. The maximization of the significance lead to the choice of a cut at $E^{\gamma}_{max} < 340$ MeV.
The final selection efficiency for $\phi \to \eta'\gamma$ events is $\varepsilon_{Sel} = 9.4\%$ while selection efficiency for the $\phi \to \eta\gamma$ background goes to $\simeq 6.7 \times 10^{-6}$. This results in an expected S/B ratio > 20 (90% C.L.) using the PDG'98 value for BR($\phi \to \eta'\gamma$).

Applying the selection criteria described above to the 2.4 pb^{-1}statistics of 1999 runs, we select $6^{+3.3}_{-2.2}$ $\phi \to \eta'\gamma \to 7\gamma$ events (with less than one event of background expected at 90% C.L.) and 10938 $\phi \to \eta\gamma \to 7\gamma$ events. This is the first observation of the decay chain $\phi \to \eta'\gamma \to 7\gamma$. The distributions of the $\phi \to \eta\gamma$ control sample compare very favourably with the simulations for what the variables on which the cut are set are concerned (see plot 14). This gives, for R_ϕ:

$$R_\phi = \frac{N_{\eta'\gamma}}{N_{\eta\gamma}} \frac{\varepsilon_{\eta\gamma}}{\varepsilon_{\eta'\gamma}} \frac{BR(\eta \to \pi^0\pi^0\pi^0)BR(\pi^0 \to \gamma\gamma)}{BR(\eta' \to \pi^0\pi^0\eta)BR(\eta \to \gamma\gamma)}$$

and, thus:

$$R_\phi = \left(6.8^{+3.2}_{-2.5}(\text{stat.}) \pm 0.9(\text{syst.})\right) \cdot 10^{-3}$$

where, as already discussed for the $\pi^+\pi^-\gamma\gamma\gamma$ final state, since most of the systematic effects cancel out in the ratio, the systematic error is dominated by the efficiency for low energy photons (10%), by

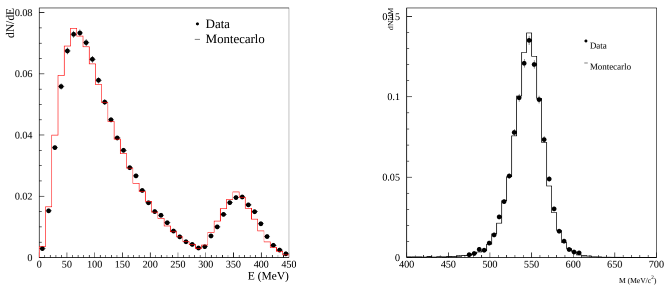

Figure 14: Monte Carlo (pure $\phi \to \eta\gamma$ sample) versus data for 7γ events: Cluster energy spectrum (left); η invariant mass (right)

the uncertainty on the value of the intermediate branching ratios (6%) and by a 5% systematic effect evaluated on the efficiency of the χ^2 cut due to radiative photon misassignment. It is interesting to note that the analysis performed in this channel, although being statistically less accurate than the one for charged/neutral final state, is fully compatible with that one, and constitutes the first measurement of R_ϕ performed with a decay chain different from the one leading to the $\pi^+\pi^-\gamma\,\gamma\,\gamma$ final state.

2.6.3 The $\eta - \eta'$ mixing angle

The importance of the measurement of R_ϕ to extract with great precision the pseudoscalar mixing angle has been stressed many times during the years (14). If one neglects $\phi - \omega$ mixing and SU(3) breaking effects in the effective Lagrangian, the $\phi \to \eta\gamma$, $\phi \to \eta'\gamma$ decays may be described as simple magnetic dipole transition, giving for the ratio R_ϕ the value:

$$R_\phi = \cot^2 \varphi_P \left(\frac{p_{\eta'}}{p_\eta}\right)^3$$

with $\varphi_P = \vartheta_P + \arctan\sqrt{2}$. In a recent paper by Bramon et al.(24) it has been stressed, however, that if one takes into account also $\phi - \omega$ mixing angle $\varphi_V = +3.4^\circ$, and accounts for SU(3) breaking via a term proportional to $\frac{m_s}{\bar{m}} \simeq 1.45$ the formula above gets a correction factor:

$$R_\phi = \cot^2 \varphi_P \left(1 - \frac{m_s}{\bar{m}}\frac{\tan\varphi_V}{\sin 2\varphi_P}\right)^2 \left(\frac{p_{\eta'}}{p_\eta}\right)^3$$

The formula above has been used, together with the measured value of R_ϕ to extract a measurement for ϑ_P , giving:

$$\vartheta_P = \left(-18.9^\circ {}^{+3.6^\circ}_{-2.8^\circ}(\text{stat.}) \pm 0.6^\circ(\text{syst.})\right)$$

3 $\phi \to \pi^+\pi^-\pi^0$

$\pi^+\pi^-\pi^0$ events are selected requiring a prompt vertex with two opposite sign tracks and two prompt photons in the calorimeter. From the two tracks, the direction of the missing momentum can be evaluated and associated with the π^0 direction. The opening angle between the two photons in the π^0 rest frame

Parameter	Fit result	PDG result
$M(\rho_0)$ (MeV)	776.1 ± 1.0	$776.0 \pm 0.9^*$
ΔM (MeV)	-0.5 ± 0.7	0.1 ± 0.9
$\Gamma(\rho)$ (MeV)	145.6 ± 2.2	150.9 ± 2.0
A(direct term)/A($\rho\pi$)	0.10 ± 0.01	$-0.15 \div 0.11$
fase(direct term)-fase($\rho\pi$)	$(114 \pm 12)^o$	

Table 5: Results of the fit to the Dalitz plot compared to the PDG values.

is required to be larger than 170^o. Furthermore in order to remove a residual background mainly due to $e^+e^-\gamma\gamma$ an opening angle between the two tracks less than 170^o is also required.

The final sample (330000 events) has been analyzed by means of the Dalitz-plot method.

The Dalitz-plot binned in 8×8 MeV squares and corrected for the efficiency is fitted to a model of $\pi^+\pi^-\pi^0$ production including the following terms:

1. $A_{\rho\pi}$ is the $\rho\pi$ amplitude given by the sum of the three ρ charged states, each described by a Gounaris-Sakurai parametrization. Free parameters are the ρ masses and the width;

2. A_{direct} is the direct term contribution given by a complex number that is two free parameters, namely a modulus and a phase. The modulus is normalized in such a way that a value equal to 1 corresponds to a direct term equal to the $\rho\pi$ term.

3. $A_{\omega\pi}$ is the $\omega\pi$ term, where mass and width of the ω are fixed to the PDG values, and only a complex amplitude that is a modulus and a phase is let free.

The fitting function is then given by (X and Y are two Dalitz variables):

$$f(X,Y) = |\vec{p}^{\,+} \times \vec{p}^{\,-}|^2 \cdot |\mathbf{A}_{\rho\pi} + \mathbf{A}_{\mathbf{direct}} + \mathbf{A}_{\omega\pi}|^2$$

where the square of the vector product in front takes into account the vector nature of the decaying particle.

In Table.5 the results of the fit are shown and compared with PDG values. Two observations can be done.

First we observe a sizeable direct term (about 10 % of the $\rho\pi$ term) with a phase respect to $\rho\pi$ loosely close to 90^o. We remark that this is the first observation of this decay.

Second we find values of the ρ line-shape parameters that are in agreement with PDG numbers. The mass is in agreement with the one obtained in e^+e^- experiments. Furthermore the mass difference between the neutral and the charged ρs is compatible with 0, so that no isospin violations are observed. The latter results improves the PDG values.

References

[1] S. Bertolucci for the Kloe collaboration, hep-ex/0002030

[2] J. Weinstein and N. Isgur, Phys. Rev. Lett. 48 (1982) 659

[3] F. Close, N. Isgur and S. Kumano, Nucl. Phys. B389 (1993) 513

[4] R. L. Jaffe, Phys. Rev. D19 (1977) 267

[5] R. L. Jaffe, hep-ph/0001123

[6] R. R. Akhmetshin et al., Phys.Lett.B462 (1999) 371; R. R. Akhmetshin et al., Phys.Lett.B462 (1999) 380

[7] M.N.Achasov et al., Phys.Lett.B479 (2000) 53; M.N.Achasov et al., hep-ex/0005017

[8] V. V. Anisovich et al., Phys. Lett. B323 (1994) 33

[9] C. Amsler et al., Phys. Lett. B333 (1994) 277

[10] N. G. Deshpande, G. Eilam, Phys. Rev. D 25 (1982) 270

[11] M. Benayoun et al., Z. Phys. C65 (1995) 399

[12] D. A. Geffen, W. Wilson, Phys. Rev,Lett. 44 (1980) 370

[13] T. Oshima, Phys. Rev. D 22 (1980) 707

[14] J. L. Rosner, Phys. Rev. D 27 (1983) 1101

[15] P. Ball et al., Phys. Lett. B365 (1996) 5611

[16] R. R. Akhmetshin et al., Phys.Lett.B473 (2000) 337

[17] M.N.Achasov et al., hep-ex/9910063

[18] R.R. Akhmetshin et al.: Phys.Lett. B434 (1998) 426

[19] F.Ambrosino, A.Denig, S.Miscetti, KLOE Memo in preparation.

[20] B.Valeriani "Studio del processo $e^+e^- \to \pi^= \pi^- \gamma$ con il rivelatore KLOE a DAΦNE, Thesis, Università degli Studi di Pisa (1999)

[21] R. R. Akhmetshin et al., hep-ex/9906032 (1999)

[22] F.Scuri, KLOE Memo in preparation

[23] F.Ambrosino, "Study of ϕ meson radiative decays with the KLOE experiment at DAΦNE " PhD Thesis , Università degli Studi di Napoli "Federico II" (1999)

[24] A.Bramon et al., Eur.Phys.J.C7 (1999) 271

[25] V.M.Aulchenko et al., JETP Lett. 69 (1999) 97

[26] R. R. Akhmetshin et al., Phys.Lett. B473 (2000) 337